Effect of activated carbon on the enhancement of CO sensing performance of NiO

A.A. Khaleed[1], A. Bello[1], J. K. Dangbegnon[1], D. Y. Momodu[1], M.J. Madito[a], F.U. Ugbo[1], A. A. Akande[2], B. P. Dhonge[2], F. Barzegar[1], O Olaniyan[1], B. W. Mwakikunga[2] and N. Manyala[1]

[1] *Department of Physics, Institute of Applied Materials, SARCHI Chair in Carbon Technology and Materials, University of Pretoria, Pretoria 0028, South Africa*

[2] *DST/CSIR National Centre for Nano-Structured Materials ,Council for Scientific and Industrial Research, P.O. Box 395, Pretoria 0001, South Africa*

Corresponding authors: N. Manyala (ncholu.manyala@up.ac.za) and B. W. Mwakikunga (bmwakikunga@csir.co.za)

Highlights

- Use of reflux technique for the production of NiO/AC composite materials.
- NiO synthesized exhibited spherical morphology.
- Composite revealed a homogeneous coating of NiO on the AC.
- Composite electrodes produced good CO sensing performance.

Abstract

NiO/activated carbon (AC) composites were successfully synthesized via a hydrothermal reflux process as an electrode material for carbon monoxide (CO) gas sensor application. The X-ray diffraction (XRD) analysis was used to investigate the crystallinity of the samples while gas sorption analysis was used to probe the specific surface area of both the pristine NiO and NiO/AC composite. The sensors were subjected to continuous cycles of different CO concentrations and were purged with air after each cycle, followed by variations in a normalized resistance study. The results obtained from the gas sensing analysis disclose that the incorporation of AC into NiO increased the conductivity and surface area of NiO/AC

composite and subsequently enhancing the CO sensing performance of NiO/AC based sensor. These results imply that the NiO/AC composite could be an excellent nanomaterial for CO gas sensors.

Introduction

In recent years, there has been exponential growth in research activities dealing with nanoparticles for resistive gas sensing applications. This is because of the high demand for simple, responsive and stable electronic sensors suitable for environmental monitoring in industries, air pollution control, safety at mining sites and firefighting. [1]. Different materials including metal/metal oxide nanoparticles, inorganic semiconductors, and carbon nanoparticles have been explored as potential materials for resistive gas sensing applications [2–8].

Metal oxides (MOs) nanomaterials have drawn a great deal of interest in gas sensing application owing to their low-cost, high surface to volume ratios, excellent sensitivity, structural stability, and good mechanical flexibility [9–11]. Nickel oxide (NiO), a p-type semiconductor with a wide bandgap of ~4 eV has been extensively investigated for diverse applications including gas sensing [12–17], supercapacitors [18,19], lithium ion batteries [20], solar cells [21,22], chemical sensing [23], electrochromic applications [24,25] and solar harvesting [26,27]. Nonetheless, MOs in general and NiO, in particular, have limited conductivity, which in turn leads to their underperformance for most of the applications mentioned above. Thus, integrating them with carbon nanomaterials can enhance their chemi-resistive gas sensing performances [1,28].

Activated carbons (AC), are well studied and have been established for utilization in many gas separation processes. Regardless of their sp^3 hybridization which makes them amorphous they still show some structural properties which are advantageous and could influence their gas sensing application [29–31]. For example, AC possesses a highly formed inner porous structure, large specific surface area, rich surface chemistry, chemical stability, the possibility of molding their structure for specific applications and most importantly they are low-cost carbon when compared to other forms of carbon such as CNT [32,33]. Furthermore, the precursor, the synthesis technique, parameters and the conditions applied during the preparation determine the chemical and structural properties of AC, which in turn could affect the adsorptive properties.

In this work, we report on the hydrothermal synthesis of NiO/AC composite and study of its CO gas sensing properties. The aim of this work is to investigate the role of activated carbon on sensing properties of NiO when exposed to industrial pollutant gasses including CO in which the composite shows the highest response. Coincidentally CO sensing has become paramount because CO molecules are dangerous to human species and could be very harmful to the environment if not properly monitored since we live in a world with very common sources of CO. The results obtained suggest that incorporation of AC in NiO/AC sensor increases its conductivity and surface area and accordingly improve its sensing performance towards CO gas when compared with the NiO sensor. Hence, NiO/AC composite holds a great potential in CO gas sensing application.

Experimental

Materials

Nickel nitrate hexahydrate ($Ni(NO_3).6H_2O$, purity 97.0%) was purchased from Sigma-Aldrich, South Africa, urea (purity 98%) was purchased from Merck, South Africa, ethanol absolute (99.9% purity) was purchased from associated chemical enterprises, South Africa. The activated carbon was obtained from Protechnik South Africa. De-ionized water (resistivity 18.2 MΩcm) from a Milli-Q Water System (Millipore Corp. Bedford, MA, USA) was used during the preparation processes.

Synthesis of NiO/AC

The synthesis procedure is similar to our previous work on $Ni(OH)_2$/GF composite [34]. Briefly, 14.884 *g* of $Ni(NO_3).6H_2O$ and 12.3002 *g* urea were dissolved in 0.16 *l* of deionized water followed by adding 50 *mg* of AC to the solution. The solution was stirred for 15 minutes to achieve a uniform and homogeneous dispersal of AC in the mixture followed by sonication for 12 h. Subsequently, the mixture was placed into 250 ml flask with a reflux condenser and immersed in an oil bath heated to 150 $^{\circ}$C with constant magnetic stirring for 2 h. Subsequently, the flask was immediately taken out from the oil bath and allowed to cool naturally. Afterward, the greenish precipitate obtained was centrifuged, washed with deionized water before drying at 80 $^{\circ}$C for 12 h in an electric oven. Lastly, the sample was calcined at 400°C in air for 1 h to obtain the NiO/AC composite material. For comparison, pure NiO was synthesized by similar procedure without the addition of AC.

The probable growth mechanism of spherical NiO with flowerlike structure could be elucidated based on the following reactions [34–36]:

$$CO(NH_2)_2 + H_2O \longrightarrow 2NH_3 + CO_2 \quad (1)$$

$$Ni^{2+} + x\,NH_3 \longrightarrow [Ni(NH_3)_x]^{2+} \quad (2)$$

$$[Ni(NH_3)_x]^{2+} \longrightarrow Ni^{2+} + x\,NH_3 \quad (3)$$

$$NH_3 + H_2O \longrightarrow OH^- + NH_4^+ \quad (4)$$

$$Ni^{2+} + 2OH^- \longrightarrow Ni(OH)_2 \quad (5)$$

$$Ni(OH)_2 \longrightarrow NiO + H_2O \quad (6)$$

Primarily, urea decays to NH_3 and CO_2 (Equation 1). Subsequently, NH_3 developed complexes with Ni^{2+}that decreases the number of free Ni^{2+} and accordingly lower the growth rate of the crystals [35,37]. Furthermore, during the hydrothermal reflux process urea can serve as a source of OH^- ion supplied by hydrolysis (equation 1 and 4). This supports the growth and nucleation of $Ni(OH)_2$ nanoparticles based on the coalescence process. Although the surface energy of distinct $Ni(OH)_2$ nanoparticle is very high, the total surface energy is reduced as the reaction prolongs further and, consequently, the $Ni(OH)_2$ nanoparticles join with each other to form flowerlike $Ni(OH)_2$ [35,37]. Following the calcination at 400 ˚C, the flowerlike $Ni(OH)_2$ spheres are degenerated to yield flowerlike NiO spheres.

Material Characterization

Powder X-ray diffraction (XRD) technique was employed to determine the crystallinity of the samples using XPERT-PRO diffractometer in a Θ/2Θ configuration, with a cobalt tube at 35 kV

and 50 mA (PANalytical BV, Netherlands). The vibrational mode analysis of the samples was carried out by a Fourier transform infrared (FT-IR) spectra (Bruker Vertex 77 v FT-IR spectrometer) operated with the OPUS software. Gas sorption analyses were carried out at −196 °C using a Micromeritics TriStar II 3020 (version 2.00) analyzer. All the samples were degassed at 90 °C for 24 h under high vacuum conditions. The surface area was calculated by the Brunauer–Emmett–Teller (BET) method from the adsorption branch in the relative pressure range (P/P_0) of 0.01 – 1. The surface morphology of the samples was studied by a field emission scanning electron microscopy (FESEM) using high-resolution Zeiss Ultra Plus 55, operating at 2.0 kV. The elemental composition of the samples was studied using an integrated energy dispersive X-ray unit from a high-resolution Zeiss Ultra plus 55, operating at 20 kV. Electron micrograph and selected area diffraction patterns of the composite were collected using High-resolution transmission electron microscopy (HR-TEM) JEOL 2100 (from Tokyo Japan) equipped with LaB6 filament, a Gartan U1000 camera of2028 x 2028 pixels and operated at 200 kV.

Gas Sensing Measurement

NCSM-CSIR gas sensing station supplied by KENOSISTEC UHV and Thin Film Equipment, Italy were used for the gas sensing measurements. The sensors were made by dispersing the materials in ethanol and ultrasonicated for 5 minutes. The resulting thick paste was carefully drop cast on the alumina sensing strip with interdigitated Pt electrodes and dried at 60 ^{o}C in an electric oven for 1 h. Lastly, the gas sensing measurements were taken by monitoring a change in electrical current for various concentration of the target gas using KEITHLEY pico-ammeter system and converted to resistance using ohms law. The gas sensor response (S) is defined as

$S = R_{in}/R_{out}$, and response percentage $S_p = S \times 100$, where R_{in} and R_{out} are the resistances of the sensor material in the presence and absence of the target gas, respectively [16,38,39]. A time taken for the resistance to achieve 90% of its final value after introduction of the target gas is called response time (T_{res}), whereas recovery time (T_{rec}) is defined as the time taken for the resistance to return to 90% of its initial value after removal of the target gas [38,40,41].

Results and Discussion

Structural and Morphological Analysis

XRD patterns of as prepared and calcined samples are presented in Fig. 1. The XRD analysis was carried out using a cobalt source (Co-K1α) with a wavelength of 1.7890 Å. Fig. 1a shows the XRD pattern of the as-prepared $Ni(OH)_2$ consisting of both hexagonal α- and β- phases of $Ni(OH)_2$. The diffraction peaks relating to the α-phase at 2Θ values of 14.08° and 28.5° are allocated to (003) and (006) planes (JCPDS No. 38-715), whereas the peaks at 2Θ values of 39.4°, 70.39° are related to β- phase and were assigned to the (101), and (110) planes (JCPD No 74-2075), respectively. After annealing at 400˚C, the as-prepared $Ni(OH)_2$ transformed to NiO with detectable reflections indexed to the cubic NiO phase (JCPDS No. 047-1049). The characteristic peaks at 2Θ values of 43.54°, 50.71°, 74.56° were assigned to (111), (200), and (220) diffraction planes of cubic NiO, respectively. Using Scherrer's equation, the average crystallite sizes for $Ni(OH)_2$ and NiO estimated from the most strong diffraction peaks (003) and (200) are 15.06 nm and 17.81 nm, respectively. The observed increase in grain sizes of NiO could be due to the coalescence effect which increases the grain size with the calcination temperature since the sufficient calcination temperature could move grain boundaries. Fig. 1b displays the XRD

diffraction patterns of $Ni(OH)_2$/AC and NiO/AC composites. The composites have similar diffraction patterns with that of pristine $Ni(OH)_2$ and NiO. No additional peaks related to the presence of carbon is observed in the $Ni(OH)_2$/AC and NiO/AC composites. This is due to the amorphous nature of AC used, as shown in the inset to Fig. 1b, resulting in broad carbon peaks with a very low intensity which overlaps with the $Ni(OH)_2$ and NiO peaks. Using the highly intense diffraction peaks (003) and (200), the average crystallite sizes calculated for $Ni(OH)_2$/AC and NiO/AC samples are 10.95 nm and 13.00 nm, respectively. The inter-planar-spacing of 2.413 Å was calculated using Bragg's equation from (111) plane of NiO/AC. Thus, the presence of AC reduces the particle size of both $Ni(OH)_2$ and NiO in the composites.

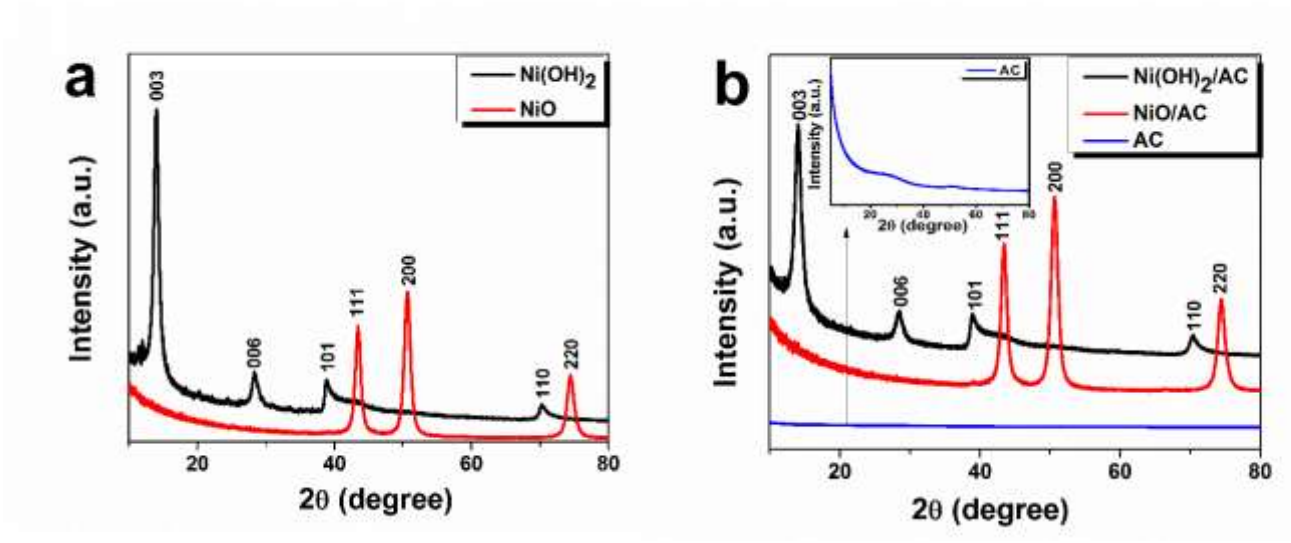

Fig. 1. XRD patterns of (a) $Ni(OH)_2$ and NiO and (b) $Ni(OH)_2$/AC and NiO/AC (inset to the figure is the XRD pattern of AC).

FTIR was used to study the vibrational modes of the samples before and after calcination as shown in Fig. 2 to confirm the transformation of $Ni(OH)_2$ to NiO. The FTIR spectra of $Ni(OH)_2$ and NiO were investigated in a wavenumber between 400 - 4000 cm^{-1}. The Peak at 3634 cm^{-1} in

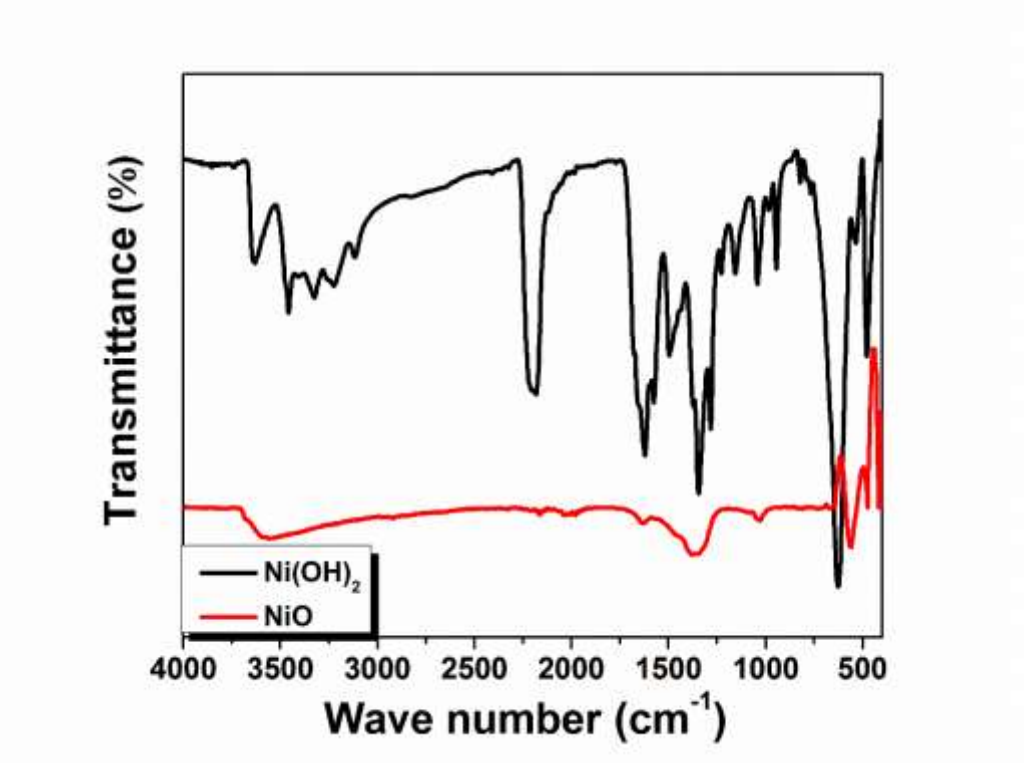

Fig. 2. FTIR spectra of the $Ni(OH)_2$ and NiO samples.

$Ni(OH)_2$ spectrum is allocated to the υ_{O-H} stretching mode [42]. Peaks at 3458 cm^{-1} and 3606 cm^{-1} are assigned to –OH stretching mode of the adsorbed water molecules for $Ni(OH)_2$ and NiO, while the absorption peaks at 1618 cm^{-1} and 1629 cm^{-1} are ascribed to the bending mode of interlayer water molecules for $Ni(OH)_2$ and NiO respectively [42,43]. The absorption peak at ~2181 cm^{-1} is ascribed to the vibration of C≡N triple bond in the OCN^{-1}, resulting from a by-product of urea hydrolysis [44]. The vibrational modes between ~1498 and 1037 cm^{-1} in both

spectra are ascribed to the presence of carbonate ions due to the interaction effect between CO_2 from the air and the samples [44–46]. The band at 1342 cm^{-1} in $Ni(OH)_2$ spectrum relates to the vibration of NO_3^- anion with D_{3h} symmetry in the interlayer space [42], while the vibrational peaks at 1282 and 945 cm^{-1} are connected to the C-N bond [47]. The bands at 623 and 478 cm^{-1} in $Ni(OH)_2$ spectrum are assigned to the δ_{OH} and υ_{Ni-OH} lattice modes [48,49]. The two peaks at 559 and 474 cm^{-1} in NiO spectrum are related to Ni–O stretching vibration, implying the presence of the crystalline NiO [46].

BET surface area and good pore size distribution (PSD) of sensor materials are vital material properties that significantly influence their gas sensing capabilities. Therefore, these properties were studied using N_2 physisorption and the result is shown in Fig 3. Fig 3a displays a type III N_2 absorption-desorption isotherms for NiO with H3 hysteresis loop, showing non-rigid accumulates of plate-like particles without saturation, while Fig. 3b display type V N_2 absorption- desorption isotherms for NiO/AC composite with H1 hysteresis loop, signifying narrow distribution of comparatively uniform pores. NiO/AC composite exhibited a higher specific surface area (69.91 $m^2 g^{-1}$) than the NiO (32.95 $m^2 g^{-1}$), this increase in the surface area in NiO/AC composite could be as a result of addition of AC and change in its morphology when compared to that of NiO as will be observed in the SEM images presented later in this work. The average pore size distribution of the two samples are similar and centered at ~10 nm (inset of Fig 3a and 3b), signifying that the samples consist of a combination of mesoporous and macroporous structures. Nevertheless, the larger BET surface area of NiO/AC composite will provide more active sites for adsorption of CO molecules, thereby improving its CO sensing performance as compared to that of NiO.

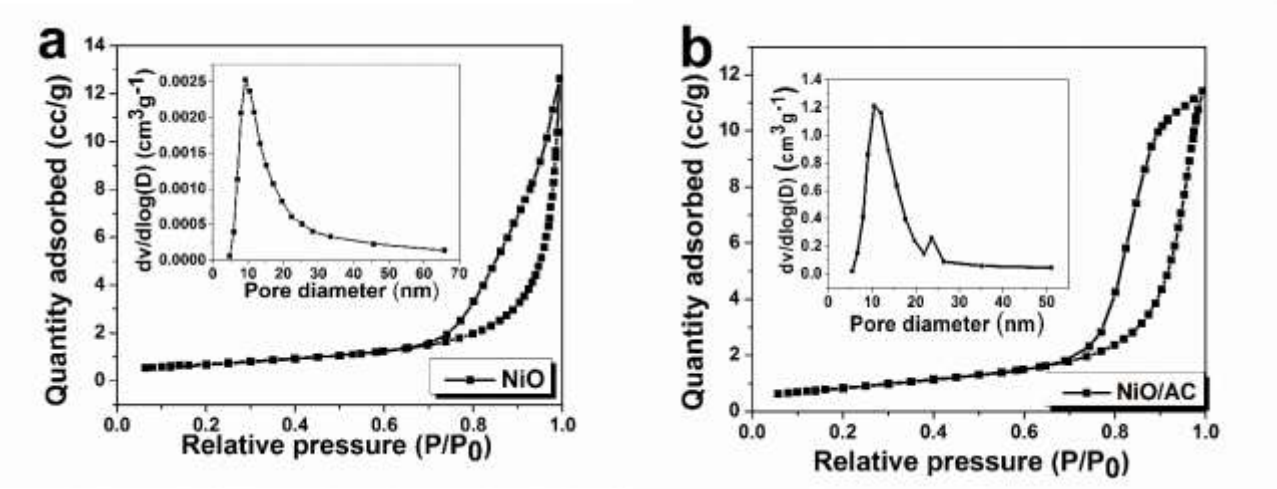

Fig 3. N_2 adsorption/desorption isotherms of (a) NiO and (b) NiO/AC. The inset presents BJH pore size distributions.

Fig. 4 illustrates low and high magnification FESEM images of NiO and NiO/AC. Spherical NiO with flowerlike nanostructures was observed at low and high magnification micrographs (Fig 4a and b). Figs. 4c and 4d show the low and high magnification SEM images of the AC. From these images, some unevenness and some seeming macropores are seen. Figs 4e and 4f displays that NiO nanoparticles has successfully cover the whole surface of the AC in the NiO/AC composite, hence, developing into a porous and electro-conductive structure. This implies that the NiO/AC composite can be a good candidate for chemi-resistive gas sensing application, owing to its higher BET surface area, good conductivity and morphology as observed from SEM images.

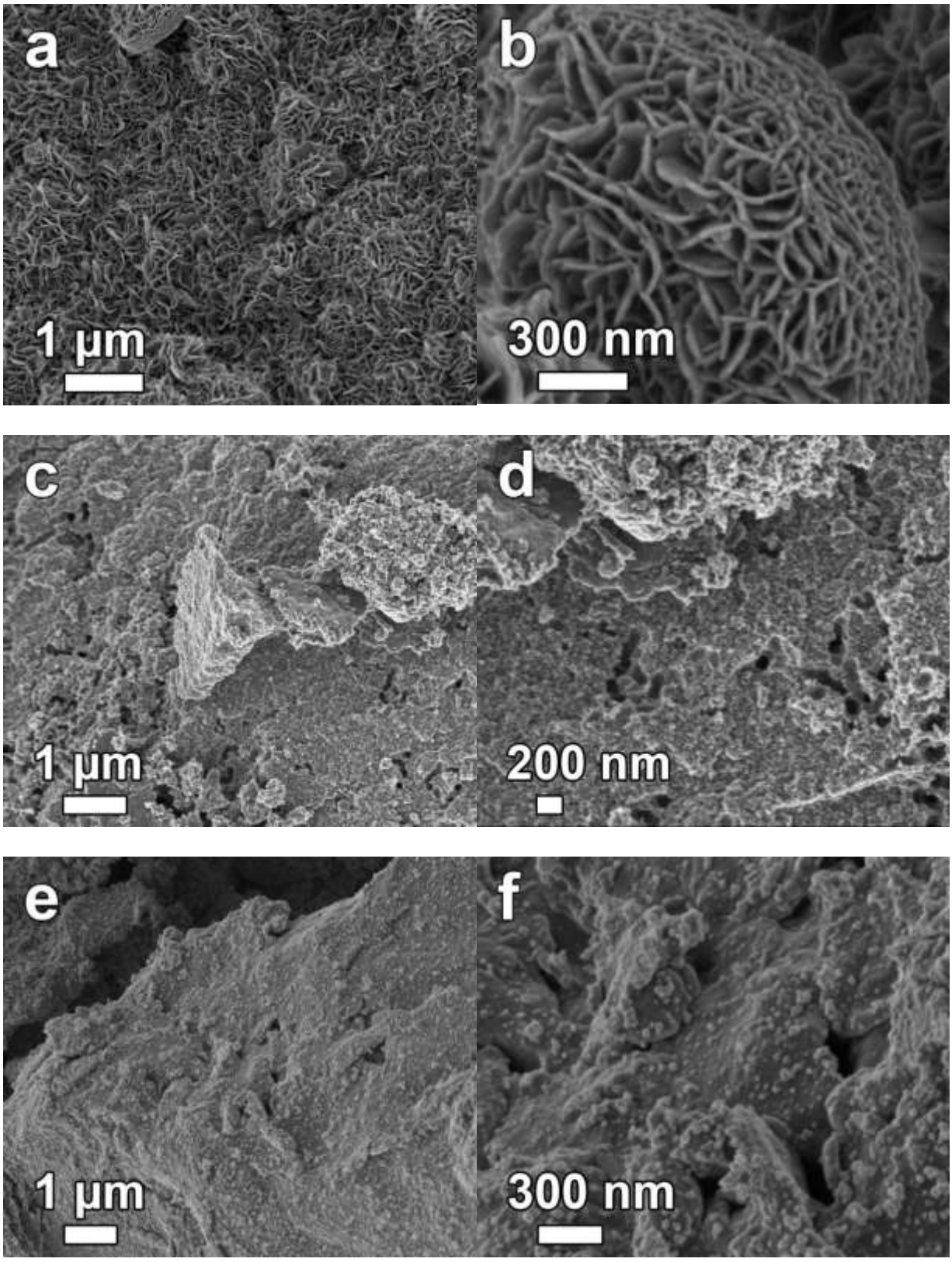
a
1 μm
b
300 nm
c
1 μm
d
200 nm
e
1 μm
f
300 nm

Fig. 4. (a) and (b) low and high magnification FESEM image of the NiO, (c) and (d) low and high magnification FESEM image of AC, (e) and (f) low and high magnification FESEM image of NiO/AC.

Fig. 5 displays the EDX spectrum of NiO/AC sample which reveals the existence of nickel, oxygen, and carbon representing the distinctive composition elements of NiO/AC. The presence of gold in the spectrum is as a result of the gold coating of the sample and aluminum is an impurity coming from the gold line during the coating process.

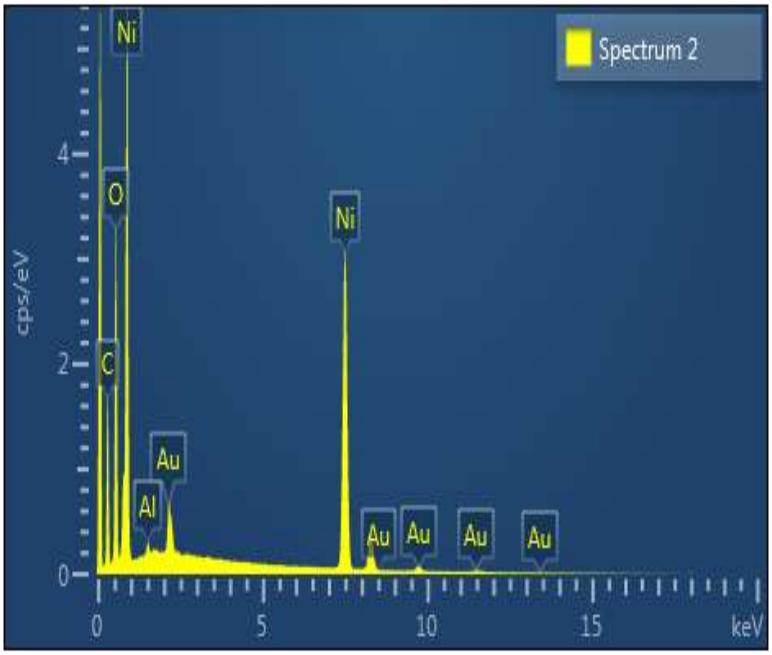

Fig. 5. EDX spectrum of NiO/AC composite

The high resolution TEM (HRTEM) micrographs of AC/NiO composite (Fig. 6) reveals the morphological and structural details of as-prepared AC/NiO composite. Fig. 6a reveals that the NiO nanostructure is anchored on the surface of the activated carbon as in indicated in the

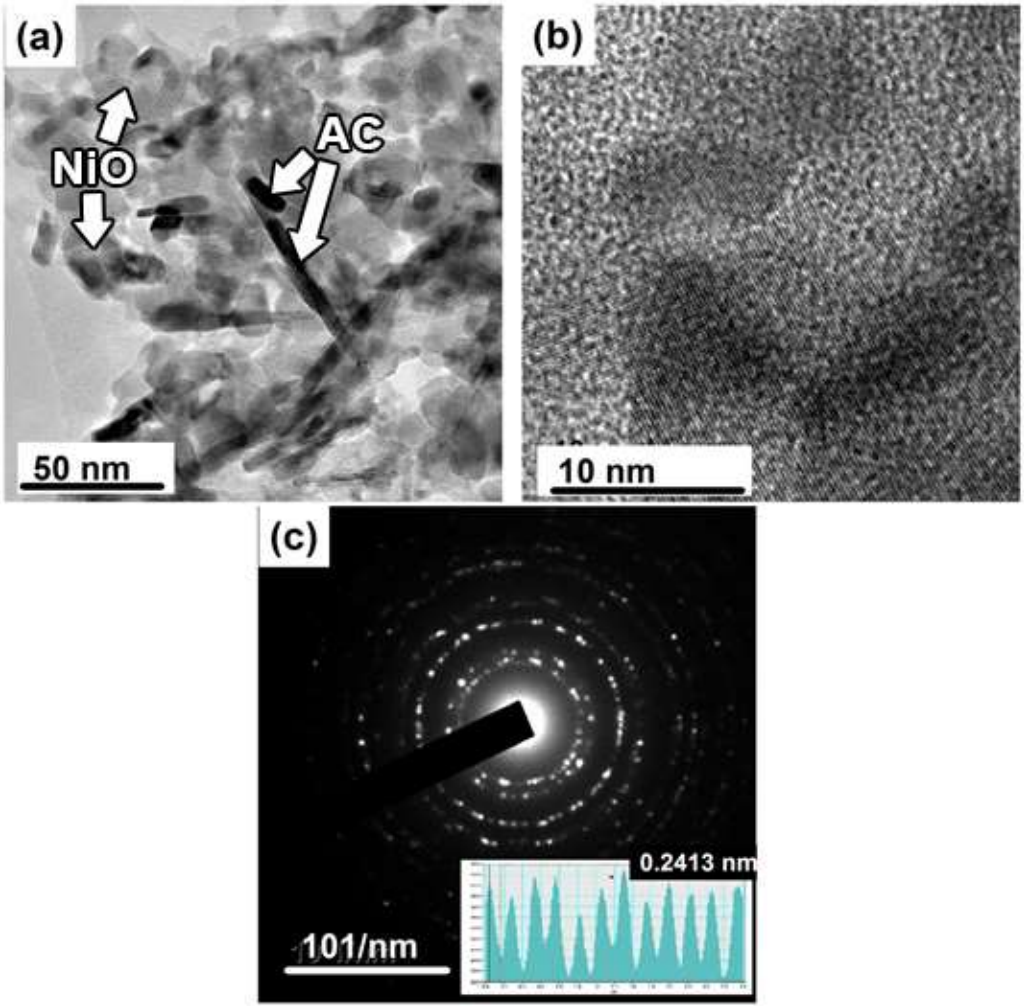

Fig. 6. An HRTEM micrograph of AC/NiO composite taken at (a) lower and (b) higher magnification and the corresponding (c) selected area electron diffraction pattern with diffraction intensity profile (inset to the figure) showing the average inter-planar-spacing.

figure, whereas nanostructured crystallites of the composite are observed in Fig. 6b, showing number of lattice fringes in different directions. The selected area electron (SAED) diffraction pattern of the composite (Fig. 6c) shows clear diffraction rings and this combined with lattice fringes having different directions confirms the polycrystalline nature of the material which is in agreement with the XRD data. The diffraction intensity profile (inset to the Fig. 6c) reveal the

average inter-planar-spacing of 2.413 Å which correspond to the (111) plane of NiO as in the XRD data.

Gas Sensing Analysis

The gas sensing properties of NiO and NiO/AC sensors were tested for CO at operating temperature of 100 ˚C. A typical p-type semiconducting behavior with respect to CO was observed from the resistance-time curves of NiO and NiO/AC sensors at different CO concentrations (5 - 100 ppm) as presented in Fig 7a and 7b. The CO gas sensing mechanism can be explained in the following reactions [11,50]:

$$O_2\,(gas) \longrightarrow O_2\,(ads) \quad (7)$$

$$O_2\,(ads) + 2e^- \longrightarrow 2O^-\,(ads) \quad (8)$$

$$1/2O_2\,(ads) + 2e^- \longrightarrow O^{2-}\,(ads) \quad (9)$$

$$CO\,(gas) + O^-\,(ads) \longrightarrow CO_2\,(ads) + e^- \quad (10)$$

$$CO\,(gas) + O^{2-}\,(ads) \longrightarrow CO_2\,(ads) + 2e^- \quad (11)$$

Initially, during the response, the atmospheric/synthetic air oxygen molecules adsorbed on the surface and ionized by taking electrons (equation 8 and 9) from the valence band create the holes. The CO molecules introduced to the chamber react with the chemisorbed oxygen species (O_2^-, O^- or O^{2-}) at the surface of the materials. Consequently, the electrons released by one of the absorbed chemisorbed oxygen are freed back to the valence band of the materials as demonstrated in equation 10 and 11. The recombination of an electron with holes, decreasing the number of holes in the materials causes an increase in resistance. Moreover, during the

recovery, the reversible reaction as described in equation 10 and 11 takes place due to the increase of CO vapor pressure.

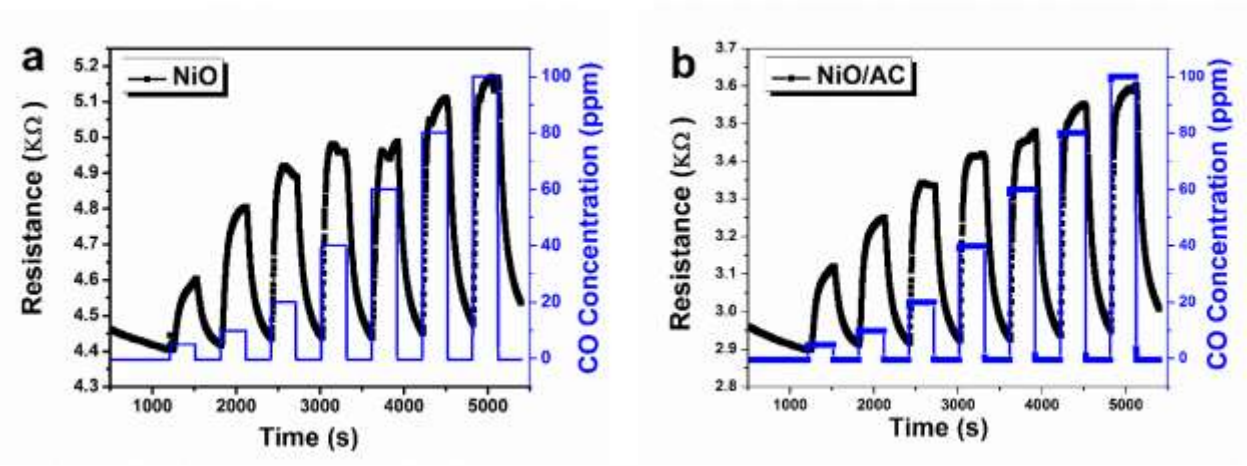

Fig 7. Resistance-time curves of (a) NiO and (b) NiO/AC sensors for different concentrations of CO at 100 ˚C**.** Note that the resistance for the pure NiO sensors is generally higher (from 4.4 kΩ to 5.2 kΩ) than that of the NiO-AC one (from 2.9 kΩ to 3.6 kΩ) demonstrating the effect that AC has on the increased conductivity in the NiO matrix.

The response percentage of both samples to CO concentration at 100 ˚C is displayed in Fig. 8a. It is observed that both NiO and NiO/AC sensors response well to CO and the gas sensor response percentage is found to be proportional to CO concentration, i.e. it increases with increase in the CO concentration. The NiO/AC sensor is observed to have higher response percentage for all CO concentrations, owing to the incorporation of AC in NiO/AC composite which improves both the electrical conductivity and surface area of the composite material, in addition to its smaller grain size and porous morphology.

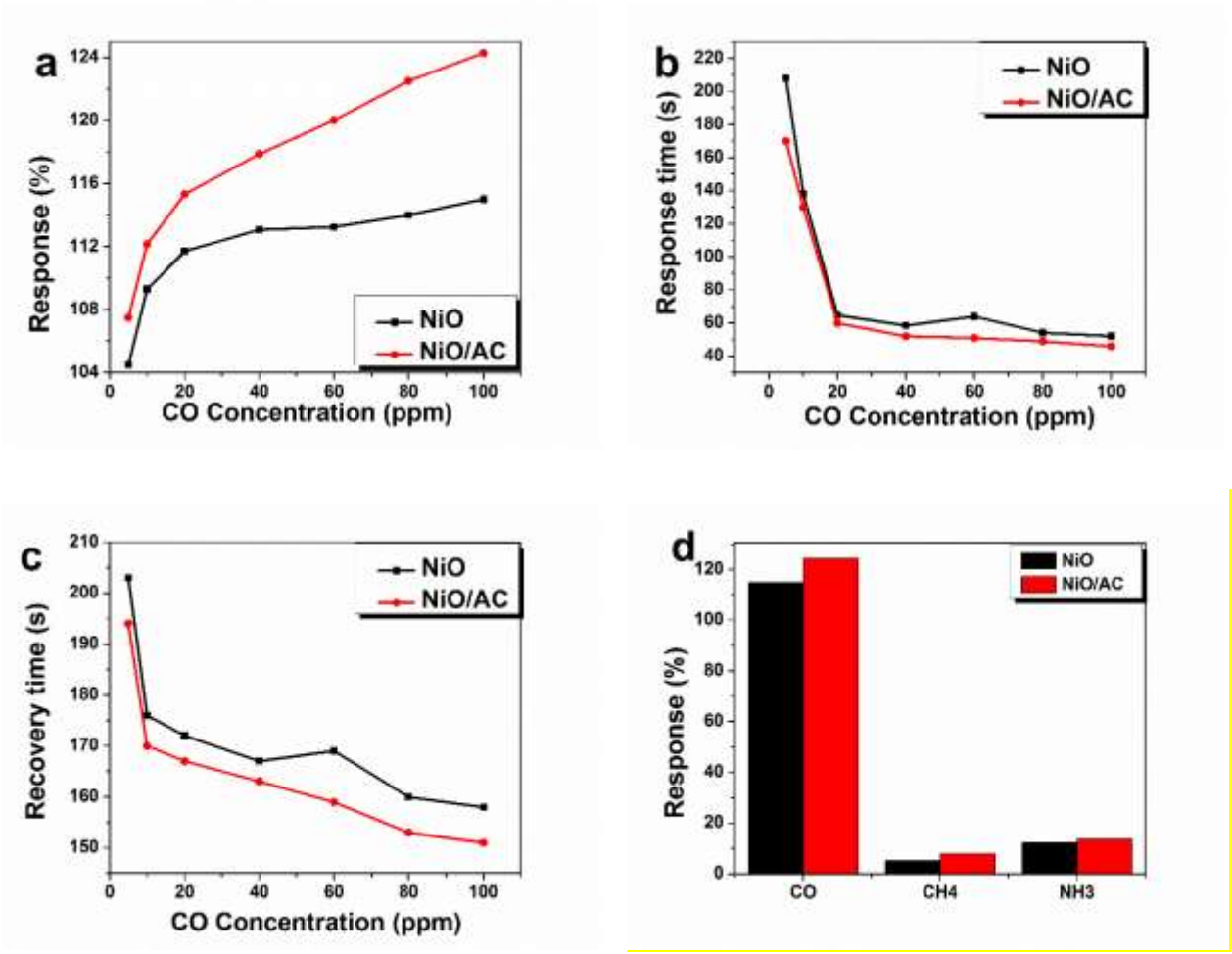

Fig. 8 (a) Sensor response of NiO and NiO/AC electrodes against CO concentration at 100 ˚C, (b) Response time of NiO and NiO/AC electrodes against CO concentration at 100 ˚C, (c) Recovery time of NiO and NiO/AC electrodes against CO concentration at 100 ˚C and (d) Selectivity of NiO and NiO/AC electrodes to 100 ppm of CO, CH_4 and NH_3 at 100 ˚C.

Response time and recovery time against CO concentration at 100 °C operating temperature are displayed in Fig. 8b and 8c, respectively. Both response and recovery time decrease with an increase in CO concentration (Fig. 8b and 8c). The decrease in response time is due to the higher pressure of striking analyte with the increase in analyte concentration [51]. Whereas,

the recovery time tends to decrease with an increase of gas concentration because the surface coverage of analyte molecules is proportionate to the analyte molecules desorption rate [52]. The smaller response time and recovery time observed for NiO/AC sensor when compared with the NiO sensor for all concentration of CO signifies that the incorporation of AC into a NiO/AC composite improves the recovery rate and enhances its CO sensing properties. Hence, AC causes NiO/AC sensor to respond higher/faster and recover faster from CO stimulus than in the absence of AC as noted in NiO sensor. It is known that response percentage, response time and recovery time depend on the adsorption and desorption rates. The increase in electrical conductivity could increase both adsorption and desorption rates thereby contributing to increase in response percentage, response time and recovery time. Whereas the increase in the surface area could only provide more adsorption sites for the gas molecules which could contribute more to response percentage, and response time since the larger the surface area of the sensor the longer it takes the gas molecules to desorb from the surface of the material causing a decrease in desorption rate. Therefore, the increase in electrical conductivity contributes more to the gas sensing performance since it could influence response percentage, response time and recovery time. Selectivity is another significant factor for assessment of a sensor. Fig. 8d displays response percentage against three reducing gasses namely CO, CH_4, and NH_3. As observed from Fig. 8d, both NiO and NiO/AC sensors have a higher response percentage to CO than CH_4 and NH_3. Thus, this confirmed their selectivity to CO compared with CH_4 and NH_3. The major preference of NiO-based sensors towards CO over NH_3 and CH_4 is due to the presence of oxygen adsorption site in the NiO-based materials which can be explained in terms of their adsorption energies. Among three aforementioned gases CO molecule has the

highest adsorption energy [53,54]. In addition to their adsorption energies, the presence of lone pair electrons in the target gasses could also influence their response percentage. CO molecule which has two lone pair electrons tends to react more with the chemisorbed oxygen species at the surface of NiO-based materials, followed by NH_3 with one lone pair electron and CH_4 lastly since it has no lone pair electrons (already saturated) that could react freely with the chemisorbed oxygen species at the surface of the NiO-based materials.

Conclusion

Hydrothermal reflux synthesis technique was successfully employed to fabricate NiO/AC sensor for CO gas sensing. The results showed that AC plays an important role in enhancing CO sensing performance of NiO since its incorporation improved on the conductivity and surface area of NiO/AC sensor as compared with the NiO sensor. Thus, the NiO/AC sensor exhibited better CO sensing performance than NiO sensor. Hence, the NiO/AC could be a future candidate for CO gas sensing application.

Acknowledgment

“This work is based on the research supported by the South African Research Chairs Initiative of the Department of Science and Technology and National Research Foundation of South Africa (Grant No 97994). Any opinion, finding and conclusion or recommendation expressed in this material is that of the author(s) and the NRF does not accept any liability in this regard”. A. A. Khaleed acknowledges financial support from the University of Pretoria and the NRF through SARChI in Carbon Technology and Materials for his Ph.D. studies.

References

[1] E. Llobet, Gas sensors using carbon nanomaterials: A review, Sensors Actuators B Chem. 179 (2013) 32–45.

[2] W. Yuan, G. Shi, Graphene-based gas sensors, J. Mater. Chem. A. 1 (2013) 10078.

[3] T. Wagner, S. Haffer, C. Weinberger, D. Klaus, M. Tiemann, Mesoporous materials as gas sensors., Chem. Soc. Rev. 42 (2013) 4036–53.

[4] L.E. Kreno, K. Leong, O.K. Farha, M. Allendorf, R.P. Van Duyne, J.T. Hupp, Metal-organic framework materials as chemical sensors., Chem. Rev. 112 (2012) 1105–25.

[5] J. Kennedy, P.P. Murmu, E. Manikandan, S.Y. Lee, Investigation of structural and photoluminescence properties of gas and metal ions doped zinc oxide single crystals, J. Alloys Compd. 616 (2014) 614–617.

[6] E. Manikandan, G. Kavitha, J. Kennedy, Epitaxial zinc oxide, graphene oxide composite thin-films by laser technique for micro-Raman and enhanced field emission study, 2014.

[7] F. Fang, J. Kennedy, J. Futter, T. Hopf, A. Markwitz, E. Manikandan, G. Henshaw, Size-controlled synthesis and gas sensing application of tungsten oxide nanostructures produced by arc discharge, Nanotechnology. 22 (2011) 335702.

[8] V. Saasa, M. Mokwena, B. Dhonge, E. Manikandan, J. Kennedy, P.P. Murmu, J. Dewer, R. Erasmus, M.F. Whaley, E. Mukwevho, B. Mwakikunga, Optical and Structural Properties of Multi-wall-carbon- nanotube-modified ZnO Synthesized at Varying Substrate Temperatures for Highly Efficient Light Sensing Devices, Sensors & Transducers. 195 (2015) 9–17.

[9] Z. Zhang, R. Zou, G. Song, L. Yu, Z. Chen, J. Hu, Highly aligned SnO_2 nanorods on graphene sheets for gas sensors, J. Mater. Chem. 21 (2011) 17360.

[10] W. An, C.Y. Yang, Progress of Research on Preparation of Micro Gas Sensors of Metal Oxide Semiconductors, Appl. Mech. Mater. 143-144 (2011) 562–566.

[11] S. Bai, W. Guo, J. Sun, J. Li, Y. Tian, A. Chen, R. Luo, D. Li, Synthesis of SnO_2–CuO heterojunction using electrospinning and application in detecting of CO, Sensors Actuators B Chem. 226 (2016) 96–103.

[12] L.T. Hoa, H.N. Tien, V.H. Luan, J.S. Chung, S.H. Hur, Fabrication of a novel 2D-graphene/2D-NiO nanosheet-based hybrid nanostructure and its use in highly sensitive NO2 sensors, Sensors Actuators B Chem. 185 (2013) 701–705.

[13] L. Wang, Z. Lou, R. Wang, T. Fei, T. Zhang, Ring-like PdO-decorated NiO with lamellar structures and their application in gas sensor, Sensors Actuators B Chem. 171-172 (2012) 1180–1185.

[14] A.M. Soleimanpour, A.H. Jayatissa, G. Sumanasekera, Surface and gas sensing properties of nanocrystalline nickel oxide thin films, Appl. Surf. Sci. 276 (2013) 291–297.

[15] W. ZENG, B. MIAO, L. LIN, J. XIE, Facile synthesis of NiO nanowires and their gas sensing performance, Trans. Nonferrous Met. Soc. China. 22 (2012) 100–104.

[16] J.-M. Choi, J.-H. Byun, S.S. Kim, Influence of grain size on gas-sensing properties of chemiresistive p-type NiO nanofibers, Sensors Actuators B Chem. 227 (2016) 149–156.

[17] J. Wang, W. Zeng, Z. Wang, Assembly of 2D nanosheets into 3D flower-like NiO: Synthesis and the influence of petal thickness on gas-sensing properties, Ceram. Int. 42 (2016) 4567–4573..

[18] A. Bello, K. Makgopa, M. Fabiane, D. Dodoo-Ahrin, K.I. Ozoemena, N. Manyala, Chemical adsorption of NiO nanostructures on nickel foam-graphene for supercapacitor applications, J. Mater. Sci. 48 (2013) 6707–6712.

[19] Z. Yang, F. Xu, W. Zhang, Z. Mei, B. Pei, X. Zhu, Controllable preparation of multishelled NiO

hollow nanospheres via layer-by-layer self-assembly for supercapacitor application, J. Power Sources. 246 (2014) 24–31.

[20] S.A. Needham, G.X. Wang, H.K. Liu, Synthesis of NiO nanotubes for use as negative electrodes in lithium ion batteries, J. Power Sources. 159 (2006) 254–257.

[21] E.A. Gibson, A.L. Smeigh, L. Le Pleux, J. Fortage, G. Boschloo, E. Blart, Y. Pellegrin, F. Odobel, A. Haqfeldt, L. Hammarström, A p-Type NiO-Based Dye-Sensitized Solar Cell with an Open-Circuit Voltage of 0.35 V, Angew. Chemie. 121 (2009) 4466–4469.

[22] K. Kaviyarasu, E. Manikandan, J. Kennedy, M. Jayachandran, R. Ladchumananandasiivam, U.U. De Gomes, M. Maaza, Synthesis and characterization studies of NiO nanorods for enhancing solar cell efficiency using photon upconversion materials, Ceram. Int. 42 (2016) 8385–8394.

[23] J. Singh, P. Kalita, M.K. Singh, B.D. Malhotra, Nanostructured nickel oxide-chitosan film for application to cholesterol sensor, Appl. Phys. Lett. 98 (2011) 123702.

[24] H. Liu, W. Zheng, X. Yan, B. Feng, Studies on electrochromic properties of nickel oxide thin films prepared by reactive sputtering, J. Alloys Compd. 462 (2008) 356–361.

[25] E. Ozkan Zayim, I. Turhan, F.Z. Tepehan, N. Ozer, Sol–gel deposited nickel oxide films for electrochromic applications, Sol. Energy Mater. Sol. Cells. 92 (2008) 164–169.

[26] K.T. Roro, N. Tile, B. Mwakikunga, B. Yalisi, A. Forbes, Solar absorption and thermal emission properties of multiwall carbon nanotube/nickel oxide nanocomposite thin films synthesized by sol–gel process, Mater. Sci. Eng. B. 177 (2012) 581–587.

[27] K.T. Roro, B. Mwakikunga, N. Tile, B. Yalisi, A. Forbes, Effect of accelerated thermal ageing on the selective solar thermal harvesting properties of multiwall carbon nanotube/nickel oxide nanocomposite coatings, Int. J. Photoenergy. 2012 (2012).

[28] M.E. Roberts, M.C. LeMieux, Z. Bao, Sorted and aligned single-walled carbon nanotube networks for transistor-based aqueous chemical sensors., ACS Nano. 3 (2009) 3287–93.

[29] N.A. Travlou, M. Seredych, E. Rodríguez-Castellón, T.J. Bandosz, Activated carbon-based gas sensors: effects of surface features on the sensing mechanism, J. Mater. Chem. A. 3 (2015) 3821–3831.

[30] M. Gonçalves, L. Sánchez-García, E. de Oliveira Jardim, J. Silvestre-Albero, F. Rodríguez-Reinoso, Ammonia removal using activated carbons: effect of the surface chemistry in dry and moist conditions., Environ. Sci. Technol. 45 (2011) 10605–10.

[31] M. Seredych, D. Hulicova-Jurcakova, G.Q. Lu, T.J. Bandosz, Surface functional groups of carbons and the effects of their chemical character, density and accessibility to ions on electrochemical performance, Carbon 46 (2008) 1475–1488.

[32] E. Frackowiak, F. Béguin, Carbon materials for the electrochemical storage of energy in capacitors, Carbon 39 (2001) 937–950.

[33] A.G. Pandolfo, A.F. Hollenkamp, Carbon properties and their role in supercapacitors, J. Power Sources. 157 (2006) 11–27.

[34] A.A. Khaleed, A. Bello, J.K. Dangbegnon, F.U. Ugbo, F. Barzegar, D.Y. Momodu, M. J. Madito, T. M. Masikhwa, O. Olaniyan, and N. Manyala, A facile hydrothermal reflux synthesis of $Ni(OH)_2$/GF electrode for supercapacitor application, J. Mater. Sci. 51 (2016) 6041–6050.

[35] J. Yan, Z. Fan, W. Sun, G. Ning, T. Wei, Q. Zhang, R. Zhang, L. Zhi, F. Wei, Advanced Asymmetric Supercapacitors Based on $Ni(OH)_2$/Graphene and Porous Graphene Electrodes with High Energy Density, Adv. Funct. Mater. 22 (2012) 2632–2641. doi:10.1002/adfm.201102839.

[36] F.-S. Cai, G.-Y. Zhang, J. Chen, X.-L. Gou, H.-K. Liu, S.-X. Dou, $Ni(OH)_2$ tubes with mesoscale

dimensions as positive-electrode materials of alkaline rechargeable batteries., Angew. Chem. Int. Ed. Engl. 43 (2004) 4212–6.

[37] H. Jiang, T. Zhao, C. Li, J. Ma, Hierarchical self-assembly of ultrathin nickel hydroxide nanoflakes for high-performance supercapacitors, J. Mater. Chem. 21 (2011) 3818–3823.

[38] B.W. Mwakikunga, S. Motshekga, L. Sikhwivhilu, M. Moodley, M. Scriba, G. Malgas, A. Simo, B. Sone, M. Maaza, S.S. Ray, A classification and ranking system on the H_2 gas sensing capabilities of nanomaterials based on proposed coefficients of sensor performance and sensor efficiency equations, Sensors Actuators B Chem. 184 (2013) 170–178. d

[39] L.-J. Bie, X.-N. Yan, J. Yin, Y.-Q. Duan, Z.-H. Yuan, Nanopillar ZnO gas sensor for hydrogen and ethanol, Sensors Actuators B Chem. 126 (2007) 604–608.

[40] C. Li, D. Zhang, X. Liu, S. Han, T. Tang, J. Han, C. Zhou, Chemical Capping Synthesis of Nickel Oxide Nanoparticles and their Characterizations Studies, Appl. Phys. Lett. 82 (2003) 1613.

[41] A. Simo, B. Mwakikunga, B.T. Sone, B. Julies, R. Madjoe, M. Maaza, VO_2 nanostructures based chemiresistors for low power energy consumption hydrogen sensing, Int. J. Hydrogen Energy. 39 (2014) 8147–8157.

[42] S. Yang, X. Wu, C. Chen, H. Dong, W. Hu, X. Wang, Spherical α-$Ni(OH)_2$ nanoarchitecture grown on graphene as advanced electrochemical pseudocapacitor materials., Chem. Commun. (Camb). 48 (2012) 2773–5.

[43] C. Nethravathi, M. Rajamathi, Chemically modified graphene sheets produced by the solvothermal reduction of colloidal dispersions of graphite oxide, Carbon 46 (2008) 1994–1998.

[44] L. Xu, Y. Ding, C. Chen, L. Zhao, 3D flowerlike α-nickel hydroxide with enhanced electrochemical activity synthesized by microwave-assisted hydrothermal method, Chem. Mater. 20 (2007) 308–

316.

[45] C. Tessier, L. Guerlou-Demourgues, Structural study of zinc-substituted nickel hydroxides, J. Mater. Chem. 10 (2000) 1185–1193.

[46] H.M. Shiri, M. Aghazadeh, Synthesis, Characterization and Electrochemical Properties of Capsule-Like NiO Nanoparticles, J. Electrochem. Soc. 159 (2012) E132.

[47] J. Lee, T. Ahn, D. Soundararajan, Non-aqueous approach to the preparation of reduced graphene oxide/α-Ni $(OH)_2$ hybrid composites and their high capacitance behavior, Chem. Commun. 47 (2011) 6305–6307.

[48] Y. Ren, L. Gao, From Three-Dimensional Flower-Like α-$Ni(OH)_2$ Nanostructures to Hierarchical Porous NiO Nanoflowers: Microwave-Assisted Fabrication and Supercapacitor Properties, J. Am. Ceram. Soc. 93 (2010) 3560–3564.

[49] X. Liu, L. Yu, Synthesis of nanosized nickel hydroxide by solid-state reaction at room temperature, Mater. Lett. 58 (2004) 1327–1330.

[50] S. Bai, S. Chen, Y. Zhao, T. Guo, R. Luo, D. Li, A. Chen, Gas sensing properties of Cd-doped ZnO nanofibers synthesized by the electrospinning method, J. Mater. Chem. A. 2 (2014) 16697–16706.

[51] A.M. Soleimanpour, A.H. Jayatissa, Effect of UV irradiation on gas sensing behavior of nanocrystalline ZnO thin films, in: 2010 IEEE Nanotechnol. Mater. Devices Conf., IEEE, 2010: pp. 225–229..

[52] H. Hu, M. Trejo, M.. Nicho, J.. Saniger, A. García-Valenzuela, Adsorption kinetics of optochemical NH_3 gas sensing with semiconductor polyaniline films, Sensors Actuators B Chem. 82 (2002) 14–23.

[53] V. Nagarajan, R. Chandiramouli, NiO nanocone as a CO sensor: DFT investigation, Struct. Chem. 25 (2014) 1765–1771.

[54] B. Wang, J. Nisar, R. Ahuja, Molecular Simulation for Gas Adsorption at NiO (100) Surface, ACS Appl. Mater. Interfaces. 4 (2012) 5691–5697.